# Single Photoelectron Spectra Analysis for the Metal Dynode Photomultiplier

February 3, 1999

**S. Tokár, I. Sýkora and M. Pikna**
Dept. of Nuclear Physics, Comenius University, Mlynska Dolina F1, 84215 Bratislava,Slovakia.
**I.Chirikov-Zorin**
Joint Institute for Nuclear Research, 141980 Dubna, Moscow Region, Russia.



**Abstract**

This note deals with a method of single photoelectron analysis suggested for the compact metal dynode photomultipliers. The spectra taken by Hamamatsu R5600 and R5900 photomultipliers have been analysed by the presented method. The detailed analysis shows that the method appropriately describes the process of charge multiplication in these photomultipliers and can be used for finding the basic internal parameters of these photomultipliers.

# 1 Introduction

Photomultipliers (PMTs) are presently widely used and will be used as light detection components of different types of scintillation detectors (counters, calorimeters, etc.). Some intrinsic spread in characteristic parameters of PMTs and their time dependence are among the most serious drawbacks of this type of light detection. Therefore a calibration and monitoring of PMT-based spectrometric channels are an inevitable and important part of the experimental setups. Especially important is the absolute calibration, i.e. the measurement of the energy deposited in scintillators in terms of photoelectrons created from the PMT photocathode and captured by the PMT first dynode. The reason is that the basic properties of the scintillating detectors (efficiency, energy resolution, etc.) depend on the amount of photoelectrons registered by a detector per unit of deposited energy. In our previous work [1] we presented a method of PMT calibration and monitoring based on deconvolution of pulse height spectra from a pulsed light source. A key point of such a method is the choice of the PMT response function. In the work mentioned above we had employed a response function suggested for high resolution PMTs with traditional structure [4] (like the PMTs with the linear focusing dynodes, box dynodes, venetian-blind dynodes) and satisfactory results had been achieved.

In this work we present the deconvolution method based on the same principles as in our method mentioned above [1], but in this case the response function is suggested for the new types of ultra compact PMTs with the metal channel dynode system [5]. The compactness of these phototubes makes them attractive for applications in high energy physics experiments where experimental setup compactness is of prime importance. The metal channel PMTs, especially the R5900, are being extensively investigated by the ATLAS collaboration for needs of the hadron calorimeter R&D program [2, 3].

# 2 Photomultiplier Response

The basic idea of the single photoelectron analysis consists of a deconvolution of the PMT pulse height spectrum and subsequent use of some of the extracted parameters for calibration and other purposes. Hence, a realistic PMT response function is a crucial point of this method. The constructed response function must take care of all substantial PMT processes. From this point of view the PMT is treated as an instrument consisting of three independent parts:

- The photodetector represented by the photocathode, where the input photon flux is converted into electrons,
- The electro-optical input system which accelerates and focuses the photoelectron flux onto the first dynode,
- The electron multiplier consisting of a series of secondary emission electrodes (dynodes), which amplifies the initial charge emitted by the photocathode.

The PMT response function must take into account peculiarities of the PMT structure, and in our case, we will concentrate on the class of metal channel dynode PMTs [5]. The global view of such a PMT is shown in Fig. 1, where the structure of a Hamamatsu R5600 PMT is depicted.

To comply with the PMT structure, a functional realization of the PMT can be divided into two independent stages. The first stage includes the photoconversion and electron collection and the second one includes the charge amplification through the dynode system.

## 2.1 Photoconversion and Electron Collection

A pulsed flux of photons incident on the PMT photocathode produces photoelectrons via the photoelectric effect. In many cases the number of photons on the photocathode is a Poisson distributed variable. In addition to this, the conversion of photons into electrons and their subsequent collection by the dynode system is a random binary process. As a result the distribution of the photoelectrons can be expressed as a convolution of Poisson and binary processes. This gives again a Poisson distribution:

$$P(n, \mu_{pc}) = \frac{\mu_{pc}^n \cdot e^{-\mu_{pc}}}{n!} \tag{1}$$

with $\mu_{pc}$ defined as

$$\mu_{pc} = n_{ph} \cdot q \tag{2}$$

where $\mu_{pc}$ is the mean number of photoelectrons collected by the dynode system,

P(n, $\mu_{pc}$) - the probability that $n$ photoelectrons will be collected provided that their mean is $\mu_{pc}$, $n_{ph}$ is the mean number of photons hitting photocathode, and $q$ is the quantum efficiency (including collection efficiency).

Note that $\mu_{pc}$ is a parameter characterizing not only the light source intensity but also the photocathode quantum efficiency and the PMT dynode collection efficiency, which depends on the voltage applied between the photocathode and the first dynode.

## 2.2 Electron Multiplication

A single photoelectron from the PMT photocathode having been focused and accelerated by the electric field, strikes the first dynode and causes a production of the secondary emission electrons. Subsequently, each of them accelerated by inter-dynode potential creates the secondary emission electrons on the second dynode, etc. For clarity the charge multiplication process in the dynode system for the R5600 PMT is shown in Fig. 2.

An electron avalanche is finally created at the anode resulting in the PMT output charge. Among the most important features of the electron avalanche is

- The emission of secondary electrons is governed by a Poisson distribution;
- The number of secondaries ($n_S$) depends on the energy ($E$) of the incident electron as $n_s = const \cdot E^{\alpha}$, where $\alpha$ is less than 1 (usually $\alpha \approx 0.4 - 0.8$) [4]);
- The energy of secondary electrons is low compared to the energy acquired from the electric field.

All these peculiarities must be considered for the response function construction. The PMT response can be easily found in the case when the number of secondary electrons on the first dynode is high ($\geq 7$ ). In this case, and in the absence of background processes, the charge distribution for the amplification process initiated by one photoelectron can be approximated by a Gaussian distribution. The distribution for the $n$ photoelectron case is a convolution of $n$ one-photoelectron distributions and a full PMT response. This idealized case is obtained by summing those with different starting numbers of photoelectrons, weighted by their occurrence probability [1]:

$$S_{ideal}(x) = \sum_{n=0}^{\infty} \frac{\mu_{pc}^n e^{-\mu_{pc}}}{n!} \frac{1}{\sigma_1 \sqrt{2\pi n}} \exp\left(-\frac{(x - nQ_1)^2}{2n\sigma_1^2}\right) \tag{3}$$

where $Q_1$ is the average charge in the one-photoelectron case and $\sigma_1$ is the standard deviation of the one-photoelectron distribution (in $n = 0$ case the limit ($n \to 0$) delta function $\delta(x)$ should be taken instead of Gaussian).

## 2.3 Realistic PMT Response Function

The basic drawbacks of the function (3) are the following:

- No background processes are taken into account;
- The one-photoelectron function is assumed Gaussian ( not true for low values of the secondary emission coefficient on the first dynode);
- No additional processes connected with semi-transparency of the photocathode (like photoelectric effect on the first dynode, focusing and acceleration electrodes) are assumed.

All these issues must be resolved in the case of a realistic response function.

### 2.3.1 Background Processes

In a real PMT various background processes will always occur which will ultimately generate some additional charge (noise). Such noise signal in the anode circuit could be generated even in absence of the light signal. An additional noise component is generated in the presence of light. The possible sources of noise are: leakage current, thermoemission from the photocathode and dynodes, optical and ion feedback, external and internal radioactivity, etc. Undesired signals of low amplitude at the PMT output can also arise due to the incident light flux. The possible sources of these signals are: the photoemission from the focusing and accelerating electrodes and from the dynodes, photoelectrons missing the first dynode and its subsequent absorption by the second dynode, etc.

The background processes generate some additional charge and modify the ideal output charge spectrum (3). We shall split the background processes into two groups:

1. The low charge processes present in each event (e.g. leakage current in the PMT anode circuit, etc.) which are responsible for a non-zero width of the pedestal ( the output charge distribution in the case when no photoelectrons were created);
2. The discrete processes, which can, with non-zero probability, accompany the real signal.

Note that by the real signal we mean the one corresponding to non-zero number of photoelectrons created from the photocathode and collected by the first dynode.

### 2.3.2 Response Function for the Metal Package PMT

To create a realistic PMT response function a few natural assumptions will be made.

1. The low charge background processes are presented, which will lead to the finite width of pedestal:

$$S_{ped}(x) = \frac{1}{\sqrt{2\pi}\sigma_0} \exp\left(-\frac{(x-Q_0)^2}{2\sigma_0^2}\right) \tag{4}$$

   with $Q_0$ - the pedestal position and $\sigma_0$- it's standard deviation.

2. The incident light can create photoelectrons from the PMT photocathode, as well as from the first dynode with the occurrence probability for $n$ photoelectrons created from the photocathode and $k$ photoelectrons created from the first dynode given by (1) and the mean number of photoelectrons: $\mu_{pc}$- from the photocathode and $\mu_1$- from the first dynode.

3. If one or two photoelectrons are collected by the first dynode, then the PMT response is expressed as a sum of responses of secondary electrons created on the first dynode, and for zero and greater than two photoelectrons collected, it is a Gaussian:

$$S_n^{(1)}(x) = \begin{cases} \sum_{m=0}^{\infty} \frac{K_1^m \cdot e^{-K_1}}{m!} \cdot S_m^{(2)}(x) & n = 1 \\ \sum_{m=0}^{\infty} K_1^m e^{-2K_1} \cdot S_m^{(2)}(x) \cdot \sum_{l=0}^{n} \frac{1}{(m-l)!l!} & n = 2 \\ G\left(x,\, Q_0 + nQ_1,\, \sigma_0^2 + n\sigma_1^2\right) & n = 0,\, n \geq 3 \end{cases} \tag{5}$$

   Where,

- $Q_0$, $\sigma_0$ are the pedestal and its width;
- $Q_1$, $\sigma_1$ - the multiplication process parameters gain, one photoelectron response standard deviation;
- $\mu_{pc}$ - the light source intensity expressed in number of photoelectrons captured by the PMT dynode system;
- $\mu_1$ - the number of photoelectrons created on the first dynode and captured by the PMT dynode system;

- $K_1$ - the secondary emission coefficient of the first dynode;
- $S_m^{(2)}(x)$ is the PMT response for the multiplication process started by an electron from the first dynode;
- $G\left(x, Q, \sigma^2\right)$ is a Gaussian distribution with the mean value of $Q$ and dispersion $\sigma^2$:

For the response $S_m^{(2)}(x)$ the expression analogous to (5) can be written:

$$S_k^{(2)}(x) = \begin{cases} \delta(x) & k = 0 \\ \sum_{m=0}^{\infty} \frac{K_2^m\, e^{-K_2}}{m!} G\left(x,\, Q_0 + mQ_3,\, \sigma_0^2 + \sigma_3^2\right) & k = 1 \\ G\left(x,\, Q_0 + kQ_2,\, \sigma_0^2 + \sigma_2^2\right) & k \geq 2 \end{cases} \tag{6}$$

where $K_2$ is the secondary emission coefficient of the second dynode, $Q_2 = Q_1/K_1$ is the mean charge at the anode initiated by one electron from the first dynode and $\sigma_2$ is corresponding standard deviation, $Q_3 = Q_2/K_2$ is the mean charge at the anode initiated by one electron from the second dynode and $\sigma_3$ is its standard deviation.

All other processes can be neglected for the moment. The output charge spectrum for the case when $n$ photoelectrons have been created on the photocathode and $k$ ones on the first dynode can be expressed as the following convolution:

$$S_{real}(x) = \sum_{n,k=0}^{\infty} \frac{\mu_{pc}^n\, e^{-\mu_{pc}}}{n!} \cdot \frac{\mu_1^k\, e^{-\mu_1}}{k!} \cdot \int dx'\, S_n^{(1)}(x') \cdot S_k^{(2)}(x - x') \tag{7}$$

The formula shown above presumes that in the case when two or less photoelectrons have been collected by the first dynode the PMT response is not a Gaussian. In this case the response is expressed as a sum of the responses corresponding to different numbers of electrons collected by the second dynode and weighted by the corresponding Poisson factors - the number of secondaries created on the dynode by one electron is governed by Poisson statistics. The convolution

$$\widetilde{S}_{nk}(x) = \int dx'\, S_n^{(1)}(x') \cdot S_k^{(2)}(x - x') \tag{8}$$

can be expressed as follows:

$$\widetilde{S}_{nk}(x) = \begin{cases} \sum_{m=0}^{\infty} \frac{K_1^m\, e^{-K_1}}{m!} G\left(x,\, Q_0 + (m+k)\cdot Q_2,\, \sigma_0^2 + (m+k)\cdot \sigma_2^2\right) & n = 1 \\ \sum_{m=0}^{\infty} K_1^m\, e^{-K_1} \sum_{l=0}^{m} \frac{1}{(m-l)!\, l!}\, G\left(x,\, Q_0 + (m+k)\cdot Q_2,\, \sigma_0^2 + (m+k)\cdot \sigma_2^2\right) & n = 2 \\ G\left(x,\, Q_0 + nQ_1 + kQ_2,\, \sigma_0^2 + n\sigma_1^2 + k\sigma_2^2\right) & n = 0,\, n \geq 3 \end{cases} \tag{9}$$

The response function $S_{real}(x)$ can be further generalized if the effect of "fly through" photoelectrons are taken into account. These are photoelectrons from the photocathode and collected on the second dynode instead of the first one. In this case the PMT response function reads:

$$S_{real}(x) = \sum_{n,k=0}^{\infty} \frac{\mu_{pc}^n\, e^{-\mu_{pc}}}{n!} \cdot \frac{\mu_1^k\, e^{-\mu_1}}{k!} \cdot \sum_{i=0}^{n} \left( \begin{array}{c} n \\ i \end{array} \right) w_2^i (1 - w_2)^{n-i} \int dx'\, \widetilde{S}_{n-i,k}(x') \cdot \widetilde{S}_i^{\,(2)}(x - x') \tag{10}$$

where

- $w_2$ is the probability that a photoelectron created on the photocathode will be captured by the second dynode (and not by the first one);
- $\widetilde{S}_i^{(2)}$is a response corresponding to i photoelectrons originating from the photocathode and collected on the second dynode.

### 2.3.3 The Limit Spectrum

For many applications it is important to consider the limit of the real spectrum (7) for high intensity light sources ($\mu_{pc} \to \infty$ ). At large values of $\mu_{pc}$ and $\mu_1$ the Poisson distributions present in (7) become Gaussian:

$$\frac{\mu_{pc}^n \exp(-\mu_{pc})}{n!} \overrightarrow{\mu_{pc} \to \infty} \frac{\exp\left(-\frac{(n-\mu_{pc})^2}{2\mu_{pc}}\right)}{\sqrt{2\pi\mu_{pc}}} \tag{11}$$

$$\frac{\mu_1^k \exp(-\mu_1)}{k!} \overrightarrow{\mu_1 \to \infty} \frac{\exp\left(-\frac{(k-\mu_1)^2}{2\mu_1}\right)}{\sqrt{2\pi\mu_1}} \tag{12}$$

and the PMT response from $n$ photoelectrons from the photocathode and $k$ photoelectrons from the first dynode can be represented by a Gaussian:

$$\widetilde{S}_{nk}(x) \overrightarrow{\mu_{pc} \to \infty} G\left(x,\, Q_0 + nQ_1 + kQ_2,\, \mu_{pc}\sigma_1^2 + \mu_1\sigma_2^2\right) \tag{13}$$

As in the summation present in (7) will effectively contribute only $n$ from $\left(\mu_{pc} - \sqrt{\mu_{pc}},\, \mu_{pc} + \sqrt{\mu_{pc}}\right)$ and $k$ from $\left(\mu_1 - \sqrt{\mu_1},\, \mu_1 + \sqrt{\mu_1}\right)$. Replacing in (7) the summation over $n$ and $k$ by integration, the PMT response function goes to the limit spectrum:

$$S_{real}(x) \overrightarrow{\mu_{pc} \to \infty} S_\infty(x) = \frac{1}{\sqrt{2\pi}\sigma_\infty} \exp\left(\frac{(x - Q_0 - Q_\infty)^2}{2\sigma_\infty^2}\right) \tag{14}$$

where

$$Q_\infty = \mu_{pc}Q_1 + \mu_1 Q_2 = \mu_{pc}Q_1\left(1 + \frac{\varepsilon}{K_1}\right) \tag{15}$$

$$\sigma_\infty = \sqrt{\sigma_0^2 + \mu_{pc}\left(\sigma_1^2 + Q_1^2\right) + \mu_1\left(\sigma_2^2 + Q_2^2\right)} \overrightarrow{\epsilon < 0.1} \sqrt{\mu_{pc}\left(\sigma_1^2 + Q_1^2\right)} \tag{16}$$

$$\tag{17}$$

where $\epsilon = \frac{\mu_1}{\mu_{pc}}$ and $K_1 \equiv$ secondary emission coefficient on the first dynode.

It is useful to find a relation between the limit spectrum parameters ($Q_\infty$, $\sigma_\infty$) and the mean number of photoelectrons ($\mu_{pc}$, $\mu_1$). From (15) and (17) it follows:

$$\mu_{pc} = f_{pmt} \cdot \frac{Q_\infty^2}{\sigma_\infty^2} \tag{18}$$

$$f_{pmt} = \frac{\sigma_1^2 + \epsilon\sigma_2^2 + Q_1^2\left(1 + \frac{\epsilon}{K_1^2}\right)}{Q_1^2\left(1 + \frac{\epsilon}{K_1}\right)^2} \quad \longrightarrow \quad 1 + \frac{\sigma_1^2}{Q_1^2} \tag{19}$$

The last relation is justified if the effect on the fisrt dynode is small ($\epsilon < 0.1$). The factor $f_{pmt}$ depends on the single photoelectron parameters (one photoelectron resolution) of the PMT in question, and its value is different from one. Typical values of $f_{pmt}$ are expected to vary between 1.15 and 1.50 .

### 2.3.4 Relation Between Amplification Process Parameters

A realistic PMT function like the one given by (7) or (10) is always expressed through several parameters characterizing the PMT: $Q_0$, $\sigma_0$, $Q_1$, $\sigma_1$, $Q_2$, $\sigma_2$, $\mu_{pc}$ and $\mu_1$ (in the case of (10) the additional parameter $w_2$ is present). Some of the parameters are clearly independent, as $Q_0$ and $\sigma_0$ ( defining pedestal position and width, $\mu_{pc}$ and $\mu_1$ - characterizing the light source intensity in combination with photon to electron conversion at the photocathode and first dynode. The other parameters $Q_1$, $\sigma_1$, $Q_2$, $\sigma_2$ , characterizing the charge multiplication

process in the dynode system, are not fully independent. It is important to know what the relationships between them are.

Starting with the assumption that the PMT has an $N$ stage dynode system and that one electron hitting the $i^{th}$ dynode will create an average $k_i$ of secondary electrons. If we denote as $Q_1$ the mean anode charge initiated by one electron captured by the first dynode, then it is easy to express $Q_1$ via dynode coefficients $k_i$ :

$$Q_1 = e \cdot k_1 \cdot k_2 \cdots k_N = e \cdot \prod_{i=1}^{N} k_i \tag{20}$$

The variance $\sigma_1^2$ of the anode charge initiated by one electron can be expressed as [6]:

$$\sigma_1^2 = Q_1^2 \left( \left( \frac{\delta_1}{k_1} \right)^2 + \frac{1}{k_1} \left( \frac{\delta_2}{k_2} \right)^2 + \ldots + \frac{1}{k_1 k_2 \cdots k_N} \left( \frac{\delta_N}{k_N} \right)^2 \right) \tag{21}$$

Where $\delta_i$ $(i = 1, \ldots, N)$ is the standard deviation of the number of secondary electrons created from the $i^{th}$ dynode by one electron.

The formulae (20) and (21) can be straightforwardly generalized for the case when the charge multiplication starts from the $j^{th}$dynode:

$$Q_j = e \cdot k_j \cdot k_{j+1} \cdots k_N = e \cdot \prod_{i=j}^{N} k_i \tag{22}$$

and

$$\sigma_j^2 = Q_j^2 \left( \left( \frac{\delta_j}{k_j} \right)^2 + \frac{1}{k_j} \left( \frac{\delta_{j+1}}{k_{j+1}} \right)^2 + \ldots + \frac{1}{k_j k_{j+1} \cdots k_N} \left( \frac{\delta_N}{k_N} \right)^2 \right) \tag{23}$$

where $Q_j$ and $\sigma_j$ are mean charge and corresponding standard deviation for the case when the charge multiplication starts from $j^{th}$ dynode.

The validity of the relation (21) is shown for the case $N = 2$ in Appendix 1 and can be easily generalized for the general case of $N$ dynodes.

Simplification of the formulae (21) and (23) can be achieved if we assume that the standard deviations $\delta_i$ are governed by a Poisson law:

$$\delta_i = \sqrt{k_i} \tag{24}$$

Assuming (24) the relation between $\sigma_j$ and $Q_j$ reads

$$\sigma_j^2 = Q_j^2 \left( \frac{1}{k_j} + \frac{1}{k_j k_{j+1}} \ldots + \frac{1}{k_j \cdots k_N} \right) \tag{25}$$

At a fixed voltage the factor in brackets is a PMT constant which can be determined as the PMT base repartition. If the repartition is $1 : 1 : \ldots : 1$ , then for all dynodes $k_i = k$ and the formula (25) becomes

$$\sigma_j^2 = Q_j^2 \left( \frac{1}{k} + \frac{1}{k^2} \ldots + \frac{1}{k^N} \right) \tag{26}$$

where $j = 1, 2, ..., N - 1$.

Now instead of 4 parameters $Q_1$, $\sigma_1$, $Q_2$, $\sigma_2$ we have only 2 independent parameters ($Q_1$, $k$). Moreover, the dynode multiplication coefficient can be found independently from the average gain G using relation:

$$G = k^N \tag{27}$$

It should be stressed that the relations like (25) and (26) are valid only for an ideal case. In a real case inhomogeneities of various kinds (like the dynode surface inhomogeneity, collection inefficiency, etc.) will make the value of standard deviation broader than in the ideal case. In our analysis we usually use three of the parameters: $Q_1$, $\sigma_1$, $k_1$ $(= Q_1/Q_2)$ finding the fourth of them on the basis of (25). On the other hand a possibility to free all four parameters has been conserved as well as a possibility to fix all possible parameters.

### 2.3.5 Secondary Emission Coefficients

The secondary emission coefficient of a dynode can be expressed [7] as

$$n = a \cdot E^{\alpha}$$

Where $E$ is the incident particle energy, $\alpha$ is a material dependent coefficient and $a$ is a coefficient determining the absolute gain of the PMT. The energy of the electron is essentially determined by inter-dynode voltage as the secondary electron is created with low energy (as compared to the energy acquired in the inter-dynode electric field). Therefore the secondary emission coefficient of the ith dynode is

$$n_i = \gamma U_i^{\alpha} = \gamma \left( \frac{U}{\sum_{j=1}^{N+1} r_j} \right)^{\alpha} r_i^{\alpha} \tag{28}$$

Where $U_i$ is the inter-dynode voltage (between dynode $i-1$ and $i$, $U$ is the overall voltage between photocathode and anode, $\alpha$ is as before and $\gamma$ is a coefficient analogous to $a$, $r_i$ $(i = 1, \ldots N+1)$ is the voltage repartition and $N$ is the number of dynodes. Using (28) the PMT gain reads

$$G = \prod_{i=1}^{N} n_i = \left( \frac{\gamma^N \cdot \prod_{i=1}^{N} r_i^{\alpha}}{\left( \sum_{i=1}^{N+1} r_i \right)^{\alpha}} \right) \cdot U^{\alpha N} \tag{29}$$

If the repartition is fixed, then the gain $G$ is an exponent function of the voltage $U$ and the formula (29) can be used to find the exponent $\alpha$.

# 3 Results of Analysis

To verify the response function we took and analyzed a series of single photoelectron spectra under different conditions. These spectra were analyzed by means of the response function (7), for two types of Hamamatsu photomultipliers: the eight dynode R5600 PMT and a ten dynode R5900 . The results of the analysis are summarized below.

## 3.1 Experimental Setup

Our analytical method based on deconvolution of the LED spectra by means of the response function (7) was tested on the experimental LED spectra. The block diagram of the experimental setup is shown in Fig. 3. An LED was used as a pulsed light source. The LED was driven by a pulse generator (GEN) with a short pulse width( $\approx 10$ *n sec* ). An optical fiber was used to tramsmit light from the LED to the PMT. The photon flux incident on the photocathode was tuned by changing the amplitude of the supply voltage to the LED. The analog signal from the PMT was amplified by a preamplifier based on the chip TL NE592D and measured by an ADC (LeCroy 2249A). The width of the LED signal was 80 *ns*. The output information from the ADC was read by means of PC computer.

## 3.2 Dependence of the Output Spectrum Parameters on the PMT Voltage.

To find the dependence of the basic PMT parameters on the voltage applied to the PMT, we had taken a series of spectra with the same pulsed light source intensity but at different high voltages. The results for the R5600 are shown in Tables 1 and 2 and in Figs. 4 and 5. In Table 1 the deconvoluted parameters of the spectra taken at different PMT voltages are shown for the case when the first dynode secondary emission coefficient $K_1$ is calculated from $Q_1$. Table 2 presents the results of analysis of the same spectra but for the case when $K_1$ is independent of $Q_1$ using the relation (22). In Fig. 4 the deconvoluted spectrum taken at $1000V$ is shown . In Fig. 5a-d the essential part of the deconvoluted spectra taken at 800 V, 850 V, 900 V and 950 V are shown in linear scale. We can clearly see from these figures the presence of the first dynode effect (the first peak after pedestal). As will be shown below,

this effect can be interpreted as caused by the photoelectric effect on the first dynode. As can be seen from Tables 1,2 and Figs. 4, 5, the parameter $Q_1$ (essentially gain expressed in the ADC channels) increases with the voltage as expected. The first dynode secondary emission coefficient $K_1$ also shows the same behavior. The small increase in the mean number of photoelectrons ($\mu_{pc}$) with voltage is seen and can be explained by the increasing collection efficiency with increasing high voltage. This effect can be especially visible for the R5600 PMT, which has a small effective photocathode, and thereby a large photocathode edge effect. From these tables we also see that the ratio $\mu_1/\mu_{pc}$ is essentially stable. The fluctuations of this ratio could stem from the systematic error in defining of the first dynode peak area. This systematic error found from the $\mu_1/\mu_{pc}$ fluctuation is about 5-7%. From the dependence of parameter $Q_1$ on the high voltage, we have found the secondary emission exponent $\alpha$. We have fit the $Q_1$ data from Table 2 with formula (29) and have obtained $\alpha = 0.874 \pm 0.007$. The result of this fit is shown in Fig. 6. The coefficient is important in the case when a non-uniform voltage repartition is applied to PMT.

Analogous dependence for the 10 dynode R5900 is shown in Table 3 and Figs. 7 and 8. Dependence of the single photoelectron parameters on voltage in the case of the R5900 was measured in two different series of measurements. The same input light intensity was used in case of the spectra taken at $780\,V$, $790\,V$ and $820\,V$. In the second series of the measurements (the spectra taken at $800\,V$ and $850\,V$) a different light intensity was applied. We see from Table 3 that in both cases the input light intensity, expressed in photoelectrons ($\mu_{pc}$), is recovered by our analysis very well. In Fig. 7 an example of the deconvoluted spectrum taken at $820\,V$ is shown and in Fig. 8 the dependence of the PMT gain $Q_1$ on voltage is shown. Latter dependences have been fit with an exponential function (29) and an exponent value of $\alpha = 0.785 \pm 0.012$ has been obtained.

### 3.3 Output Spectrum Parameters vs. First Dynode Voltage.

To understand the nature of the first dynode effect we have taken spectra with different voltages between the first dynode and photocathode ($U_1$). The voltage $U_1$ is a sensitive parameter that enables us to distinguish between the photoelectric effect and the "fly through" process. In the latter effect the photoelectron created from photocathode is captured by the second dynode instead of the first one. If the first dynode effect is caused by "fly through" electrons, then the position of the first dynode peak ($Q_2$) will move with the voltage $U_1$ as $(Q_2 \sim (U_1 + U_2)^{\alpha}$, while if it is caused by the photoelectric effect on the first dynode, then this peak will not move, as in this case $Q_2 =\sim U_2^{\alpha}$ and $U_2$ does not change. To exclude possible systematic uncertainties (determining of the first dynode peak area, etc.) we fixed the secondary emission coefficient on the first dynode peak $K_1$ via formula (28) : $K_1 = 0.088 \cdot U_1^{0.87}$. The results of analysis are presented in Fig. 9 and Table 4 from where we see that the position of the first dynode peak ($Q_2$) does not move with the voltage $U_1$. In the case of a "fly by" effect, more than 50 % increase of $Q_2$ is expected when $U_1$ is increased form 139 V to 228 V. Therefore we are justified to conclude that the first dynode peak is caused by the photoelectric effect on the first dynode. From the results we also see that the fit $\chi^2$ increases with increasing voltage $U_1$(increasing repartition non-uniformity). Fig. 9 neatly shows that the discrepancy is in the region of small amplitudes (left side of the one photoelectron distribution), where an excess is of the real events over the expected ones is observed. The discrepancy at high first dynode voltage can be caused by an edge effect: The increasing first dynode voltage can increase the collection efficiency by capturing the photoelectrons created at the edge of photocathode. Those photoelectrons may produce less secondary electrons from the first dynode and that would lead to the enhanced left tail of the one-photoelectron distribution.

## 4 Conclusions

The presented results show that the deconvolution method suggested for analysis of single photoelectron spectra of metal channel photomultiplier works well at least for the class of the above mentioned PMTs. The PMT response function employed in this method in an adequate way describes processes in the metal channel photomultiplier.

Our method enables one to find some very important PMT parameters like the position of the charge distribution initiated by 1 photoelectron ( PMT gain ), its standard deviation, etc.(c.f. part 2.3.4). On the basis of these parameters we can calculate the PMT correction factors needed for finding the correct relation between the mean numbers of photoelectrons and the anode spectrum ( 18,19 ), and enables us to calculate the energy-to-signal conversion factor (number of photoelectrons per $GeV$) for PMT based calorimeters.

The method can be used as a calibration and monitoring tool for studying the time stability of a photomultiplier using the gain (parameter $Q_1$) as a calibration parameter.

# 5 Acknowledgements

The authors want to thank R. Stanek (Argonne NAL,USA) for an accurate reading of the manuscript and for valuable remarks and Yu. Kulchitsky, I. Minashvili and V. Romanov (JINR Dubna) for technical help.

## Appendix. Fluctuations in a Two Dynode System

In the case of a two-dynode system the anode charge can be expressed as

$$q = \sum_{i=1}^{q_1} q_2^{(i)} \tag{30}$$

Where $q_1$ is the number of electrons created from the first dynode and $q_2^i$ is the number of electrons created from the second dynode by ith electron from the first dynode. The mean value of charge $q$ is easy to find:

$$\bar{q} = E\left(\sum_{i=1}^{q_1} q_2^{(i)}\right) = \sum_{m=0}^{\infty} P_m^{(1)} \sum_{i=1}^{m} E\left(q_2^{(i)2}\right) = \sum_{m=0}^{\infty} P_m^{(1)} m k_2 = k_1 k_2 \tag{31}$$

Where $E$ is the expected value, $P_m^{(1)}$ is the probability to have $m$ electrons created from the $1^{st}$ dynode. We used the fact that each of the $1^{st}$ dynode electrons creates from the $2^{nd}$ dynode the same average number of electrons $k^2$.
The dispersion $\sigma_q^2$ can be expressed as

$$\sigma_q^2 = E\left(q^2\right) - k_1^2 \dot{k}_2^2 \tag{32}$$

Where

$$\begin{aligned} E\left(q^2\right) &= E\left(\sum_{i,j=1}^{q_1} q_2^{(i)} q_2^{(j)}\right) = \sum_{m=0}^{\infty} P_m^{(1)} \sum_{i=1}^{m} E\left(q_2^{(i)2} q_2^{(j)2}\right) \\ &= \sum_{m=0}^{\infty} P_m^{(1)} \left(m\bar{q_2^2} + m(m-1)k_2^2\right) = k_1 \bar{q_2^2} + k_2^2 \bar{q_1^2} - k_1 k_2^2 = k_1 \sigma_2^2 + k_2 \bar{q_1^2} \end{aligned} \tag{33}$$

Combining (32) and (33) we have

$$\sigma_q^2 = (k_1 k_2)^2 \left[\left(\frac{\sigma_1}{k_1}\right)^2 + \frac{1}{k_1}\left(\frac{\sigma_2}{k_2}\right)^2\right] \tag{34}$$

Generalization of (34) to the general case of $N$ dynodes is straightforward and leads to the relation (21).

# 6 Tables

Table 1: Dependence of the R5600 PMT output spectrum parameters on the voltage applied to the PMT. The fitting function (7) has been applied with the ratio $\sigma_3/Q_3 = \sigma_2/Q_2$ and $K_1$ calculated from $Q_1$.

| U | 800 V | 850 V | 900 V | 950 V | 1 kV |
|---|---|---|---|---|---|
| $Q_0$ | 13.53± 0.022 | 13.59 ±0.017 | 13.59±0.015 | 13.45±0.018 | 13.54 ±0.015 |
| $\sigma_0$ | 0.47±0.017 | 0.47 ±0.015 | 0.49 ±0.015 | 0.67 ±0.02 | 0.53±0.017 |
| $Q_1$ | 15.20 ±0.04 | 23.32 ±0.09 | 35.24 ±0.26 | 50.52 ±0.37 | 72.76 ±0.63 |
| $\sigma_1$ | 7.80 ±0.16 | 11.32 ±0.23 | 16.92 ±0.31 | 24.73 ±0.47 | 32.04 ±0.60 |
| $K_1$ | 5.74 | 5.97 | 6.23 | 6.58 | 7.06 |
| $\sigma_2$ | 1.60 ±0.06 | 2.40 ±0.09 | 3.07 ±0.08 | 5.55 ±0.26 | 6.10 ±0.13 |
| $\mu_{pc}$ | 1.446 ±0.009 | 1.459 ±0.010 | 1.466 ±0.015 | 1.520 ±0.014 | 1.519 ±0.017 |
| $\mu_1$ | 0.832 ±0.035 | 0.867 ±0.03 | 0.892 ±0.025 | 0.883 ±0.024 | 0.949 ±0.023 |
| $\chi^2$ | 77.9 / 126 | 134.8 / 181 | 260.0 / 287 | 413.7/ 388 | 533.0 / 493 |
| $\mu_1/\mu_{pc}$ | 57.5 % | 59.4 % | 60.8 % | 58.1 % | 62.5 % |

Table 2: Dependence of the R5600 PMT output spectrum parameters on the voltage U applied to the PMT. The fitting function (7) has been applied with the ratio $\sigma_3/Q_3 = \sigma_2/Q_2$ and $K_1$ independent of $Q_1$.

| U | 800 V | 850 V | 900 V | 950 V | 1 kV |
|---|---|---|---|---|---|
| $Q_0$ | 13.55± 0.021 | 13.59 ±0.017 | 13.59±0.015 | 13.45±0.018 | 13.54 ±0.015 |
| $\sigma_0$ | 0.47±0.017 | 0.47 ±0.014 | 0.49 ±0.015 | 0.67 ±0.02 | 0.53±0.017 |
| $Q_1$ | 15.13 ±0.17 | 23.18 ±0.22 | 35.17 ±0.26 | 50.48 ±0.38 | 72.63 ±0.61 |
| $\sigma_1$ | 7.87 ±0.16 | 11.46 ±0.24 | 17.00 ±0.30 | 24.75 ±0.48 | 32.19 ±0.61 |
| $K_1$ | 5.53 ±0.14 | 5.97 ±0.11 | 6.23 ±0.09 | 6.58 ±0.09 | 7.06 ±0.08 |
| $\sigma_2$ | 1.62 ±0.07 | 2.46 ±0.10 | 3.10 ±0.08 | 5.92 ±0.25 | 6.16 ±0.13 |
| $\mu_{pc}$ | 1.450 ±0.023 | 1.464 ±0.019 | 1.468 ±0.015 | 1.521 ±0.015 | 1.520 ±0.012 |
| $\mu_1$ | 0.804 ±0.037 | 0.841 ±0.03 | 0.879 ±0.025 | 0.880 ±0.025 | 0.936 ±0.023 |
| $\chi^2$ | 73.9 / 125 | 125.1 / 180 | 258.2 / 286 | 413.3/ 387 | 530.6 / 492 |
| $\mu_1/\mu_{pc}$ | 55.4 % | 57.4 % | 59.9 % | 57.9 % | 61.6 % |

Table 3: Dependence of the R5900 PMT output spectrum parameters on the voltage U applied to the PMT. We assume that $\sigma_3/Q_3 = \sigma_2/Q_2$ and $K_1$ is calculated on the basis of $Q_1$.

| U | 780 V | 790 V | 800 V | 820 V | 850 V |
|---|---|---|---|---|---|
| $Q_0$ | 20.97 ± 0.020 | 20.98 ±0.020 | 14.97 ±0.020 | 20.94 ±0.02 | 14.97 ±0.013 |
| $\sigma_0$ | 0.83 ±0.012 | 0.84 ±0.012 | 0.86 ±0.026 | 0.86 ±0.011 | 0.83 ±0.007 |
| $Q_1$ | 31.82 ±0.08 | 35.71 ±0.19 | 41.15 ±0.10 | 50.13 ±0.52 | 73.04 ±0.54 |
| $\sigma_1$ | 22.86 ±0.26 | 24.67 ±0.3 | 28.16 ±0.41 | 32.48 ±0.40 | 42.13 ±0.66 |
| $K_1$ | 4.42 | 4.47 | 4.53 | 4.62 | 4.80 |
| $\sigma_2$ | 6.76 ±0.17 | 7.43 ±0.20 | 8.89 ±0.18 | 10.15 ±0.33 | 12.86 ±0.36 |
| $\mu_{pc}$ | 1.25 ±0.01 | 1.24 ±0.009 | 0.88 ±0.005 | 1.25 ±0.015 | 0.86 ±0.008 |
| $\mu_1$ | 0.140 ±0.008 | 0.149 ±0.008 | 0.103 ±0.005 | 0.142 ±0.008 | 0.106 ±0.008 |
| $\chi^2$ | 262.4 / 276 | 257.9 / 292 | 524.0 / 291 | 341.0 / 428 | 999.0 / 500 |

Table 4: Dependence of the $R5600$ PMT parameters vs. the voltage between photocathode and $1^{st}$ dynode is $U_1$ (changed from $139\,V$ to $228\,V$). The voltage between the $1^{st}$ dynode and anode was fixed at $861\,V$. $K_1$ is fixed using formula (28) with secondary emission exponent $\alpha = 0.87$ and voltage repartition: $U_1 : \ldots 115 : 115 : 55$; the last voltage in this ratio is th voltage between the last dynode and anode.

| $U_1$ | 139 V | 185 V | 205 V | 228 V |
|---|---|---|---|---|
| $Q_0$ | 11.57 ± 0.020 | 11.65 ±0.019 | 11.66 ±0.018 | 11.59 ±0.013 |
| $\sigma_0$ | 0.66 ±0.014 | 0.65 ±0.014 | 0.66 ±0.013 | 0.48 ±0.014 |
| $Q_1$ | 82.02 ±0.46 | 102.94 ±0.56 | 112.17 ±0.61 | 123.09 ±0.69 |
| $\sigma_1$ | 39.81 ±0.75 | 47.53 ±0.93 | 52.98 ±1.00 | 56.97 ±1.17 |
| $K_1$ | 6.49 | 8.32 | 9.10 | 9.98 |
| $\sigma_2$ | 8.25 ±0.15 | 10.72 ±0.17 | 12.06 ±0.17 | 12.07 ±0.14 |
| $\mu$ | 1.254 ±0.01 | 1.294 ±0.010 | 1.276 ±0.010 | 1.269 ±0.010 |
| $\mu_1$ | 0.601 ±0.013 | 0.584 ±0.013 | 0.555 ±0.013 | 0.551 ±0.014 |
| $\chi^2$ | 751.6 / 549 | 730.0 / 670 | 908.9 / 681 | 1468.6 / 732 |

# List of Figures


1 The overall view of a Hamamatsu R5600 photomultilier. . . . . 16
2 Charge multiplication process in the metal channel dynode photomultiplier. . . . . 16
3 Block scheme of the experimental setup for the measurement of single photoelectron spectra. . . . . 17
4 The deconvoluted LED spectrum taken at 1000 V by a Hamamatsu R5600 photomultilier. The first dynode secondary emission coefficient $K_1$ is treated as an independent parameter. . . . . 18
5 The deconvoluted LED spectra taken at 800 V, 850 V,900 V, and 950 V by a Hamamatsu R5600 photomultiplier. The same conditions are valid as in the case of the spectrum in Fig. 3. . . . . 19
6 Dependencies of the gain (parameter $Q_1$) for the R5600 photomultiplier. . . . . 20
7 Deconvoluted LED spectrum taken at 820 V by a Hamamatsu R5900 photomultilier. . . . . 21
8 Dependence of the gain (parameter $Q_1$) on voltage for the R5900 photomultiplier. . . . . 22
9 Deconvoluted LED spectra taken at different first dynode voltages (139 V, 185 V, 205 V, and 228V) by a Hamamatsu R5600. The voltage between the first dynode and anode was fixed at 861 V. . . . . 23

# References


[1] E.H Bellamy, I. Chirikov-Zorin, S. Tokar, et al,Absolute Calibration and Monitoring of a Spectrometric Channel Using a Photomultiplier, Nucl Instrum Meth A339,468-476(1994)

[2] ATLAS Collaboration, ATLAS Technical Proposal for a General-Purpose pp experiment at the Large Hadron Collider, CERN/LHCC/ 94-93, CERN, Geneva, Switzerland.

ATLAS Collaboration, ATLAS TILE Calorimeter Technical Design Report, CERN/LHCC/96-42, ATLAS TDR 3, 1996, CERN, Geneva, Switzerland.

[3] a) ATL-TILECAL-98-156 . (ATL-L-PN-156) . Measurement of 20 Hamamatsu R-5900 Photomultiplier Tubes for ATLAS TileCal Module-0 . by: Ames,E ; et al. - 23 Mar 1998

b) ATL-TILECAL-98-152 . (ATL-L-PN-152) . Light yield of the 1997 Extended Barrels Module 0 from Cs data with nominal PMT settings . by: S.Bravo and M.Delfino ; - 23 Mar 1998

c) ATL-TILECAL-98-148 . (ATL-L-PN-148) . Technical characteristics of the prototype of the TILECAL photomultipliers test-bench . by: M.Crouau G.Montarou D.Rey ; - 23 Mar 1998

d) ATL-TILECAL-97-131 . (ATL-L-PN-131) . Study of the light produced in PMT/light guide region of Tile barrel Module 0 . by: Henriques,A ; Nessi,M ; Poulsen,U ; - 28 Nov 1997

e) ATL-TILECAL-97-129 . (ATL-L-PN-129) . Characterization of 8-stages Hamamatsu R5900 photomultipliers for the TILE calorimeter . by: Crouau,M ; Grenier,P ; Montarou,G ; Poirot,S ; Vazeille,F ; - 20 Oct 1997

f) ATL-TILECAL-97-128 . (ATL-L-PN-128) . Addendum on the estimation of Module 0 PMT 480 nm quantum efficiency . by: G.Montarou ; - 20 Oct 1997

g) ATL-TILECAL-97-125 . (ATL-L-PN-125) . Characterization of EMI 9112A photomultipliers at Valencia for the ATLAS Tile Calorimeterby: Castillo,V ; Chiron,L ; Fassi,F ; Ferrer,A ; Gil,I ; Gonzalez,S ; Higon,E ; Romance,J.B ; - 20 Oct 1997

h) ATL-TILECAL-97-120 . (ATL-L-PN-120) . Light produced in the Fibre bundle/Light guide/PMT region of the Tile Calorimeter prototype . by: Di Girolama,B ; Henriques,A ; Maio,A ; Santos,J ; Varanda,M ; - 25 Jun 1997

i) ATL-TILECAL-97-117 . (ATL-L-PN-117) . Study of the charge spectra generated by photomultipliers . by: Cavasinni,V ; et al. - 06 Jun 1997

j) ATL-TILECAL-97-115 . (ATL-L-PN-115) . An estimation of Module 0 R5900 PMT quantum efficiency . by: Montarou,G ; - 10 Apr 1997

k) ATL-TILECAL-97-108 . (ATL-L-PN-108) . Characterization of the Hamamatsu 10-stages R5900 photomultipliers at Clermont for the TILE calorimeter . by: Bouhemaid,N ; Crouau,M ; Gil Botella,A ; Gonzalez de la Hoz ; Grenier,P ; Montarou,G ; Muanza,G.S ; Poirot,S ; Vazeille,F ; - 28 Apr 1997

l) ATL-TILECAL-96-097 . (ATL-L-PN-97) . Characterization of the new R5900 Hamamatsu photomultiplier in Pisa . by: Beschastnov, P ; Cavasinni, V ; Cologna, S ; Del Prete, T ; Di Girolamo, B ; Mazzoni, E ; - 09 Dec 1996

m) ATL-TILECAL-96-083 . (ATL-L-PN-83) . Results of test linearity of 10-stages and 8-stages R5900 PMTS . by: Crouau, M ; Garnier, E ; Montarou, G ; - 13 Sep 1996

n) ATL-TILECAL-94-041 . (ATL-L-PN-41) . The Tilecal 3-in-1 PMT Base concept and the PMT block assembly . by: Ajaltouni, Z ; et al. - 06 Dec 1994

[4] Photomultiplier Tubes, principles an applications, Philips catalog

[5] Y. Yoshizawa, J.Takeuchi, The latest vacuum photodetector, Nucl Instrum Meth A387 (1997) p. 33

[6] ATL-TILECAL-97-108 . (ATL-L-PN-108) . Characterization of the Hamamatsu 10-stages R5900 photomultipliers at Clermont for the TILE calorimeter . by: Bouhemaid,N ; Crouau,M ; Gil Botella,A ; Gonzalez de la Hoz ; Grenier,P ; Montarou,G ; Muanza,G.S ; Poirot,S ; Vazeille,F ; - 28 Apr 1997

[7] G. Barbiellini, A.Martins, F.Scuri, A simulation study of the behaviour of fine photomultipliers in magnetic field, Nucl Instrum Meth., A362(1996) p. 245

[8] Application Software Group, CERN Program Library, 1995, CERN, Geneva, Switzerland.

[9] I.S. Gradshteyn and I.M. Ryzhik, Table of Integrals, Series, and Products, 5th ed., Academic Press, 1994.

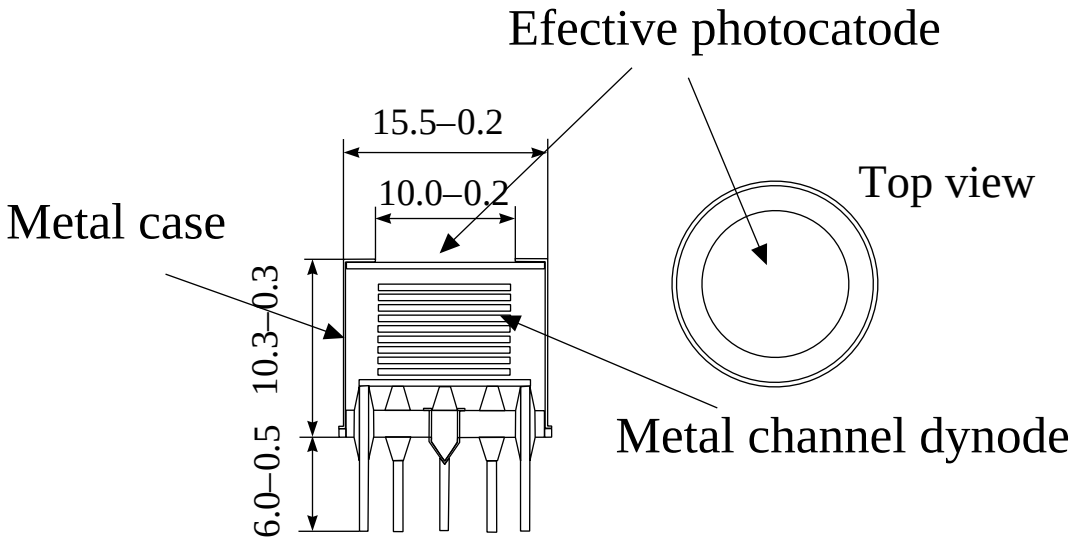


Figure 1: The overall view of a Hamamatsu R5600 photomultilier.

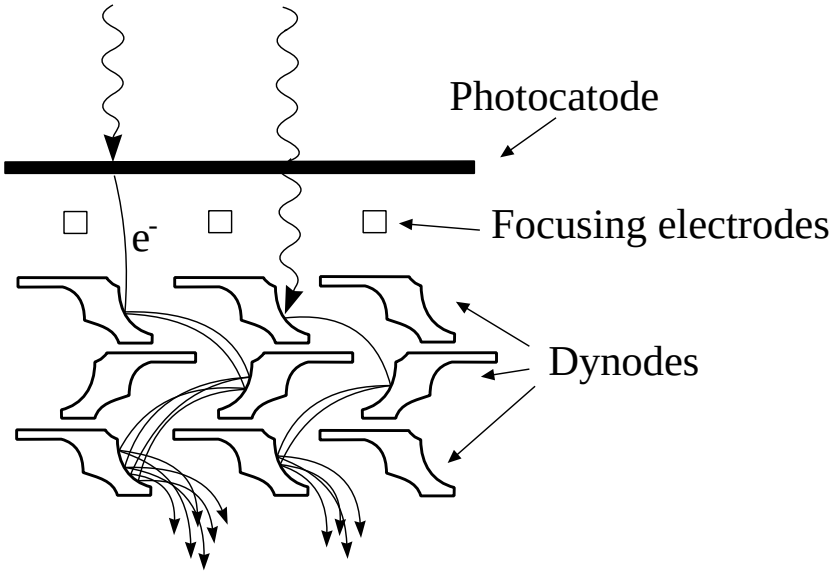


Figure 2: Charge multiplication process in the metal channel dynode photomultiplier.

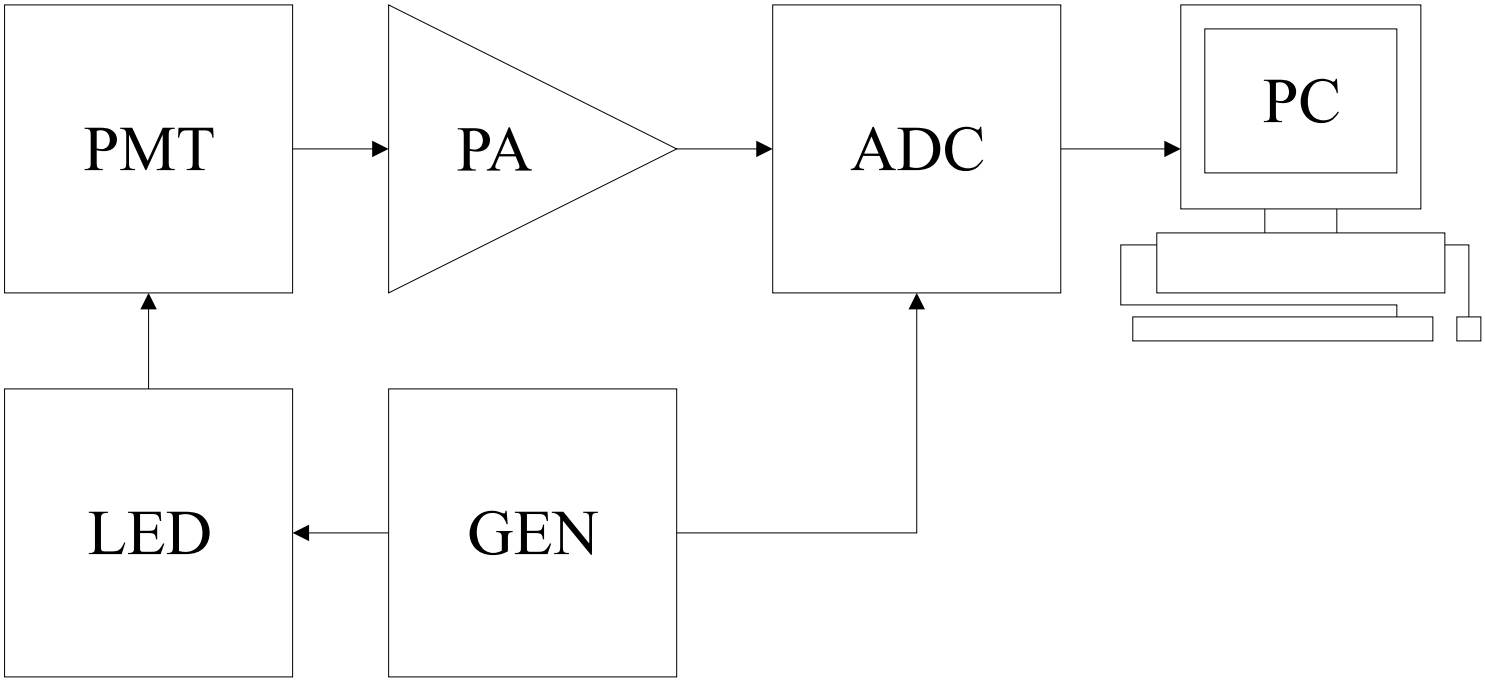


Figure 3: Block scheme of the experimental setup for the measurement of single photoelectron spectra.

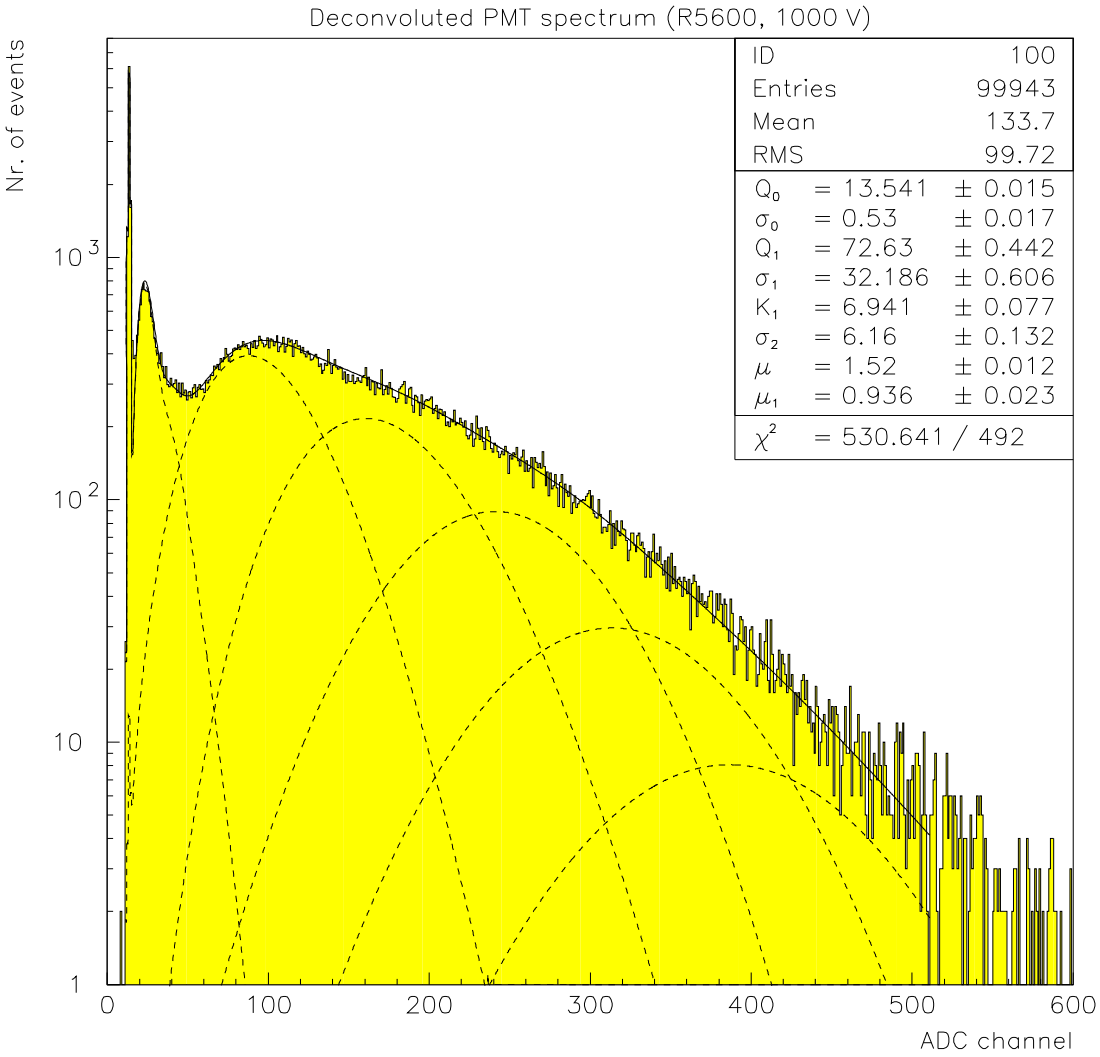


Figure 4: The deconvoluted LED spectrum taken at 1000 V by a Hamamatsu R5600 photomultilier. The first dynode secondary emission coefficient $K_1$ is treated as an independent parameter.

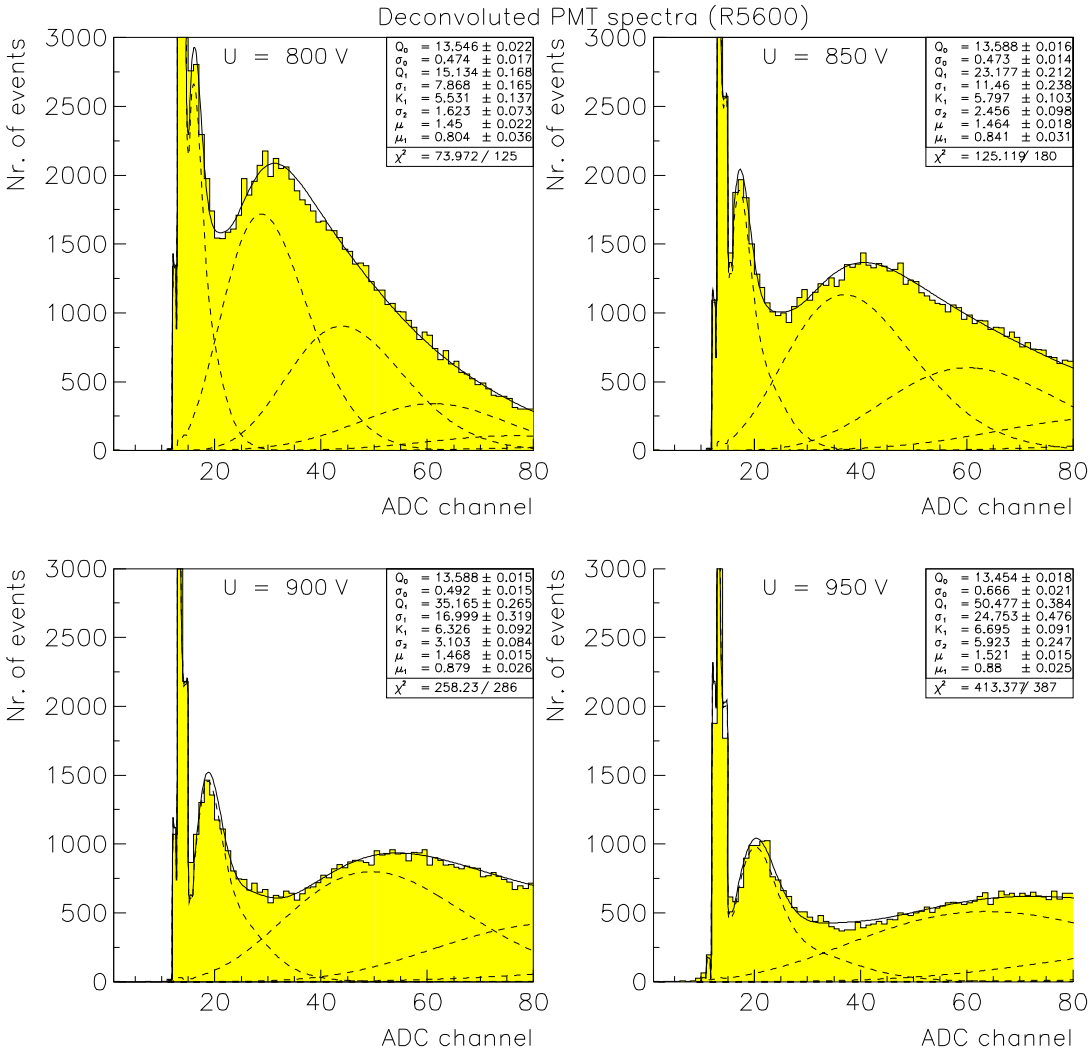


Figure 5: The deconvoluted LED spectra taken at 800 V, 850 V,900 V, and 950 V by a Hamamatsu R5600 photomultiplier. The same conditions are valid as in the case of the spectrum in Fig. 3.

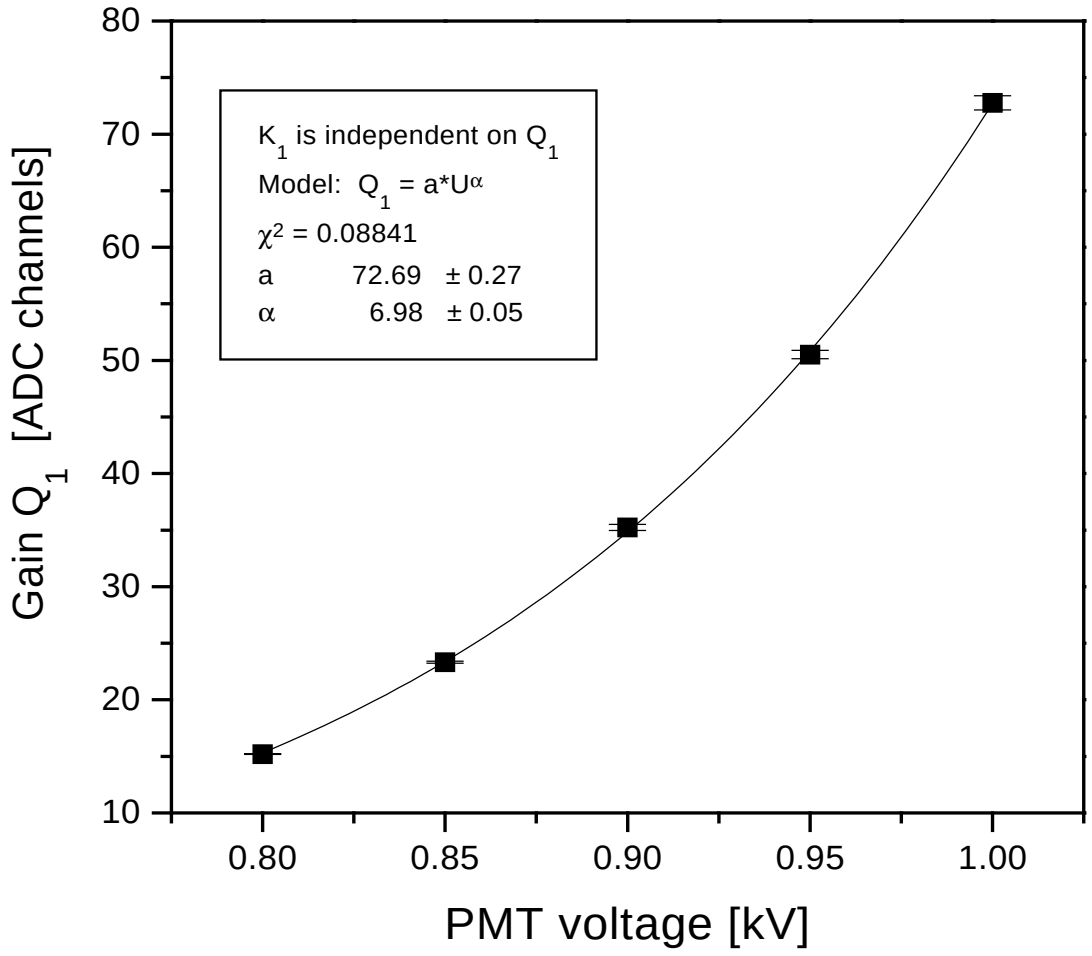


Figure 6: Dependencies of the gain (parameter $Q_1$) for the R5600 photomultiplier.

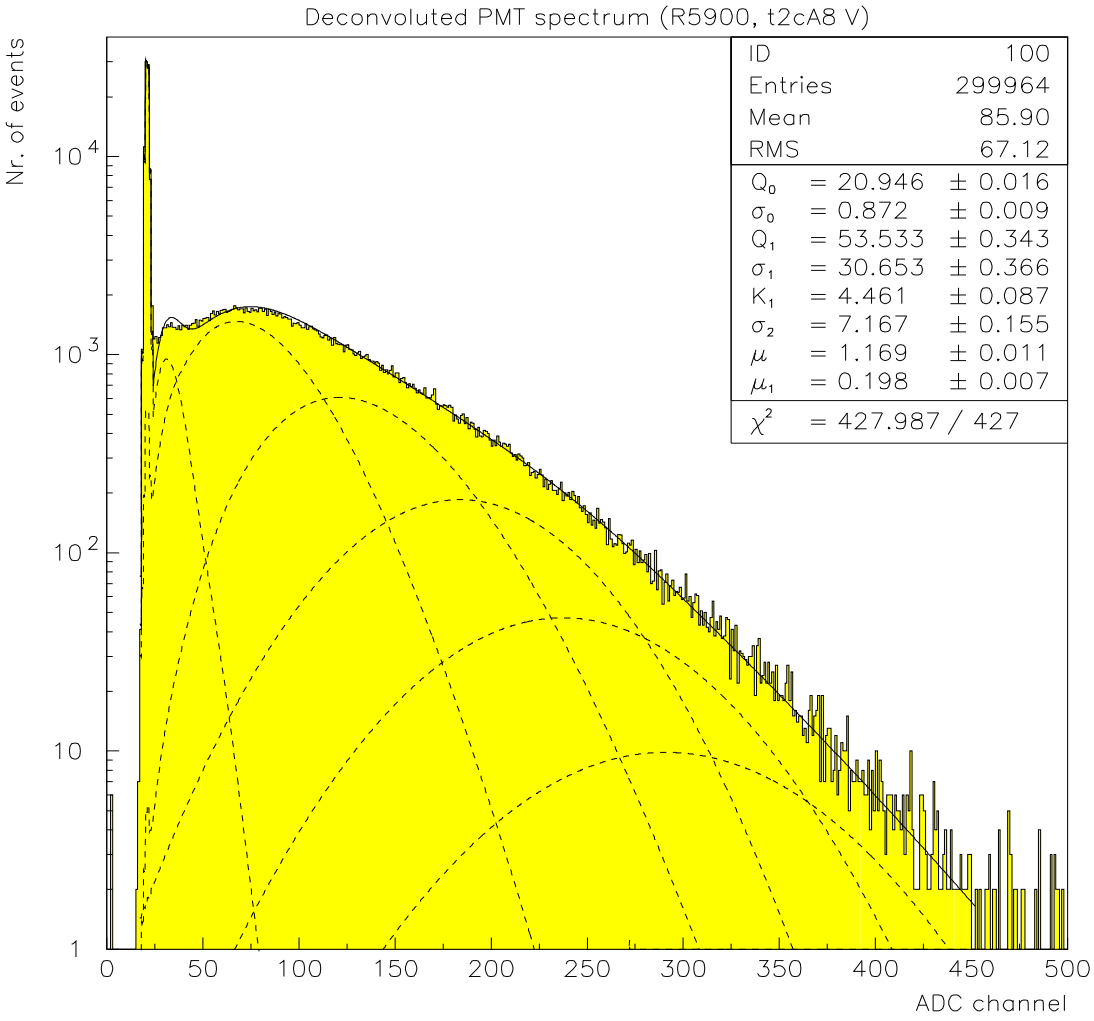


Figure 7: Deconvoluted LED spectrum taken at 820 V by a Hamamatsu R5900 photomultilier.

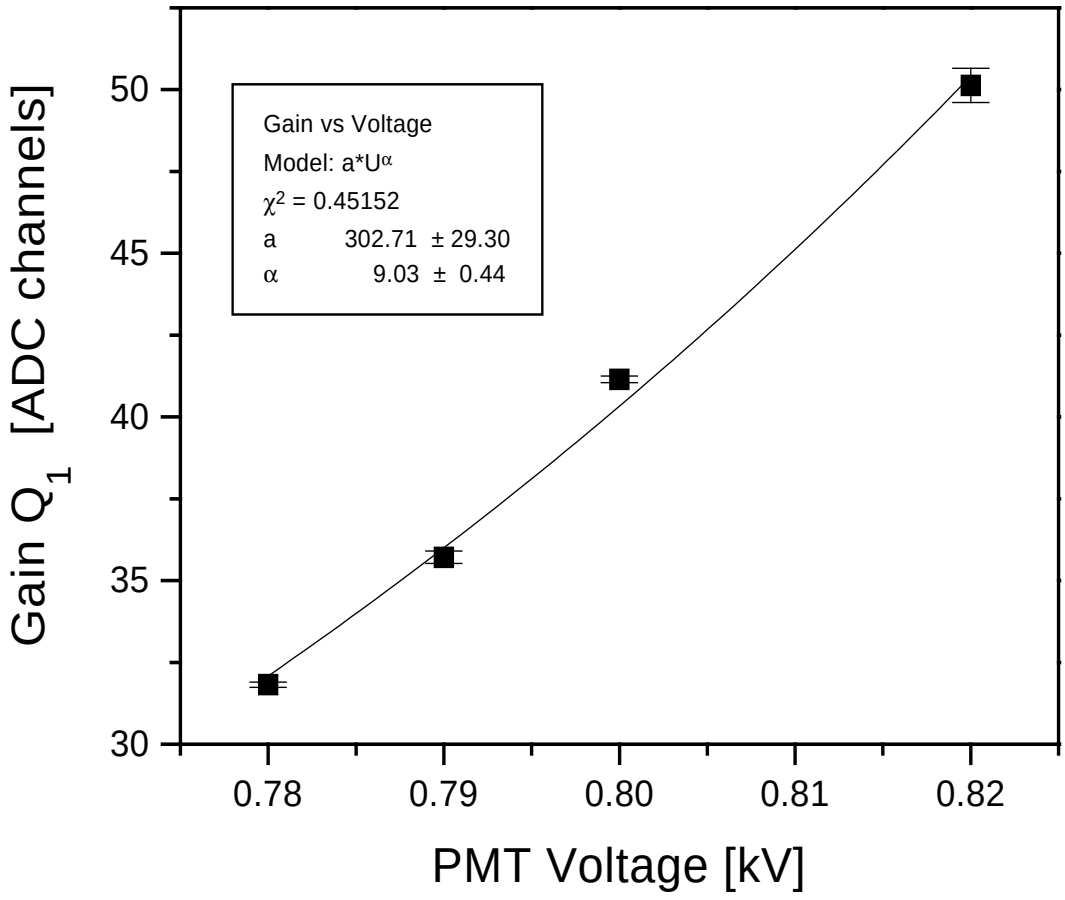


Figure 8: Dependence of the gain (parameter $Q_1$) on voltage for the R5900 photomultiplier.

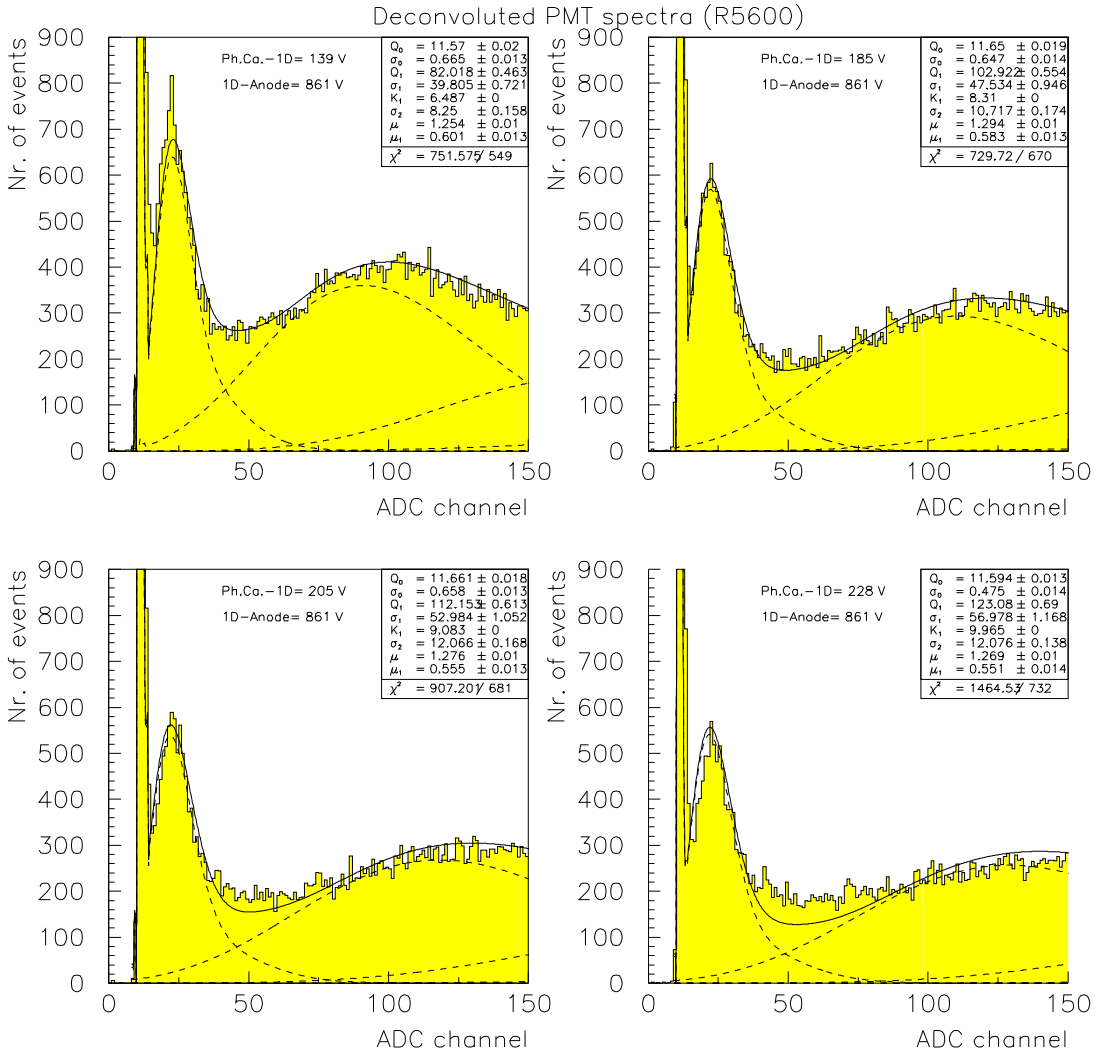


Figure 9: Deconvoluted LED spectra taken at different first dynode voltages (139 V, 185 V, 205 V, and 228V) by a Hamamatsu R5600. The voltage between the first dynode and anode was fixed at 861 V.